THE ASTROPHYSICAL JOURNAL, 281: 76–89, 1984 June 1

IUE OBSERVATIONS OF HIGH-REDSHIFT QUASARS[1]

JILL BECHTOLD, RICHARD F. GREEN, AND RAY J. WEYMANN
Steward Observatory, University of Arizona

MAARTEN SCHMIDT
Palomar Observatory, California Institute of Technology

FRANK B. ESTABROOK, RICHARD D. SHERMAN, AND HUGO D. WAHLQUIST
Jet Propulsion Laboratory, California Institute of Technology

AND

T. M. HECKMAN
Astronomy Program, University of Maryland
Received 1983 September 12; accepted 1983 December 7

ABSTRACT

We have measured the continuum energy distributions of nine high-redshift quasars ($1.0 \leq z \leq 2.2$) with the *International Ultraviolet Explorer* and the Palomar 5 m multichannel spectrophotometer. Generally, the spectral energy distributions steepen at a rest wavelength of about 1200 Å, from a power law, $f_{\nu_0} \propto \nu^{\alpha}$, in the optical, of spectral index $\alpha \approx -0.5$, to a spectral index of -3 to -5 shortward of 1200 Å. The amount of observed steepening is correlated with redshift, but not intrinsic QSO luminosity, consistent with the interpretation that it is primarily caused by absorption by intervening material. To determine the nature of this material, we have observed several of the quasars in our sample from the ground using spectrographs on the Multiple Mirror Telescope and the Steward 90 inch (2.3 m) telescope, in the region just shortward of Lyman-alpha in emission. We find that the composite effect of the observed Lyman-alpha absorption lines is adequate to account for the observed change of continuum slope near 1200 Å, when Lyman continuum opacity is considered. For reasonable values of the Lyman-alpha velocity widths ($20 \leq b \leq 50$ km s^{-1}), we find that four to eight Lyman continuum absorption edges associated with the strongest few percent of the Lyman-alpha absorption lines would then be responsible for suppressing the continuum shortward of 912 Å in the quasar rest frame. The required range of equivalent widths of Lyman-alpha coincides roughly with that in which metal absorption lines are observed, and these absorbers can probably be identified with the low column density end of the distribution of metal-containing systems, rather than the high column density end of the Lyman-alpha "forest." Reddening by our Galaxy also contributes to the observed steepening of the quasar continua but does not alter the above conclusions regarding intervening H I. Reddening intrinsic to the quasar must have only a small effect on the continuum, unless the amount of reddening is correlated with redshift, which is unlikely. While intrinsic steepening of the continuum cannot be ruled out in any particular object, the effects of reddening, and especially of intervening material, must be accurately removed before the intrinsic nature of the quasar continuum can be ascertained.

Six of our spectra exhibit a total of nine optically thick Lyman limit discontinuities with $z_{\rm abs} \ll z_{\rm em}$. Eight out of nine of the systems surveyed have associated Mg II or C IV doublets, with physical parameters consistent with the hypothesis that the absorbing material is associated with a galactic halo or disk. Combining our sample with other observations of high-z QSOs, we find that the Lyman limit systems have a statistical distribution that is well described by a population of intervening absorbers whose comoving density is constant from $z = 0.4$ to $z = 3.5$. If these absorbers are associated with galaxies, then an L^* galaxy must have a cross section to absorption corresponding to 5–10 Holmberg radii to account for the distribution we see.

Subject headings: opacities — quasars — spectrophotometry — ultraviolet: spectra

I. INTRODUCTION

With the launch of the *International Ultraviolet Explorer* (*IUE*), studies of the far-ultraviolet spectral region in high-redshift quasars have become possible for the first time (Green *et al.* 1980). Studies of QSOs down to an observed wavelength of 1200 Å, corresponding to a rest frame wavelength well below the Lyman limit, combine with observations at other wavelengths to help sketch out a complete picture of the energy distribution in QSOs from the radio to the X-rays and γ-rays. In particular, the continuum in the ultraviolet can be an important diagnostic of the physical processes occurring near the QSOs central engine, e.g., in an accretion disk (Malkan and Sargent 1982). In addition, the far-UV spectrum is important in understanding the ionization and other physical parameters of the material in the broad-line region of QSOs, the ionization history of the intergalactic medium, and the number-magnitude relations for faint blue objects.

We have observed the continuum energy distributions in nine high-redshift QSOs ($1.0 \leq z \leq 2.2$) with *IUE* and the Palomar 5 m multichannel spectrophotometer. These observa-

[1] Based on data acquired with the *International Ultraviolet Explorer* satellite, operated at the Goddard Space Flight Center for the National Aeronautics and Space Administration; the Multiple Mirror Telescope Observatory, a joint facility of the University of Arizona and the Smithsonian Institution; the Steward Observatory 90 inch (2.3 m) telescope; and the Palomar Observatory, California Institute of Technology.

tions are a continuation of the previous *IUE* work of Green *et al.* (1980) and complement similar studies of very high redshift, high-luminosity quasars observed from the ground (e.g., MacAlpine and Feldman 1982; Smith *et al.* 1981; Oke and Korycansky 1982).

II. OBSERVATIONS

Three types of data were acquired for this investigation: ultraviolet spectrophotometry, optical spectrophotometry, and optical spectroscopy. We present the observing details of each in turn.

The ultraviolet spectra were obtained with the *International Ultraviolet Explorer* satellite (Boggess *et al.* 1978*a*, *b*) by blind offset of the targets into the large (10″ × 20″) apertures. We used the line-by-line images produced from the geometrically and photometrically corrected frames by the *IUE* SIPS procedures (Turnrose and Perry 1977); we then produced a net spectrum with a five line wide extraction slit and a background found by averaging those lines that were free of reseaux and strong cosmic-ray events. Because no other smoothing filter was applied to the background, the signal-to-noise ratio appears somewhat worse than that from the standard extraction, but it reflects the discrete origin of the background level. The absolute calibration is that of Bohlin *et al.* (1980), with a quoted accuracy of about 10%. The times of observation and camera frame numbers are listed in Table 1.

Optical spectrophotometry was obtained with the multichannel spectrophotometer on the Hale 5 m telescope (Oke 1969). The objects were observed on photometric nights through a pair of 15″ apertures, with decker settings allowing 80 Å bandpasses for wavelengths from 3200 Å to 5700 Å and 160 Å bandpasses for wavelengths from 5700 Å to 1.1 μm. Integration times were typically 100 s for each of four settings for a 16th magnitude object. Absolute fluxes for each night were calibrated with reference to the observation of a single flux standard sdG star on the "AB79" system (Oke and Gunn 1983). The extinction correction was applied using a standard monochromatic extinction table for Palomar. The photon statistical accuracy for wavelengths shorter than 8000 Å was usually better than 1%, and the systematic errors are expected to be less than 2%–3%. The one exception to this scheme is PKS 0237−233, which was observed through a pair of 8″ apertures with the SIT spectrograph on the Hale 5 m. The extracted net spectrum was binned to approximate multichannel resolution.

A potential systematic error is introduced by the nonsimultaneity of the optical and ultraviolet spectrophotometric measurements. Although none of the objects is known to be a high-amplitude variable, it is probable that several cases could have a 10% discontinuity at the optical-*IUE* observational boundary (e.g., Usher, Warnock, and Green 1983). This effect should not bias the statistical results of, for example, power-law fitting, because there should be no preferred sense of variability.

The third type of observation is optical spectroscopy to search for absorption lines. These data were acquired with the Steward 90 inch telescope, Boller & Chivens spectrograph, and blue pulse-counting Reticon detector. An 832 lines mm^{-1} grating in second order afforded 1.5 Å resolution over an 1100 Å range through a pair of 2.″5 apertures. Observations of the quality shown in Figure 4 required 1–2 hr of integration and were obtained during the spring and fall observing seasons in 1982. PG 1634+706 and PG 1718+481 were observed with the Multiple Mirror Telescope, MMT spectrograph, and pulse-counting Reticon detector (Latham 1982). After being screened at 1 Å resolution, they were then observed with the MMT echelle spectrograph (Green *et al.* 1983), and the equivalent widths quoted in Table 6 are derived from those spectra.

III. DISCUSSION

a) The Continuum Energy Distribution

In Figures 1 and 2 we have plotted the spectral energy distributions of the quasars in our sample. The *IUE* spectra are binned in approximately 200 Å bands (see Table 2), and data within 10,000 km s^{-1} of prominent emission lines—Lyα, C IV, Mg II, C III], Si IV–O IV, He II, O VI–Lyβ, and C III]–Lyγ—have been deleted. Each spectrum has been converted to the quasar's rest frame, where

$$\nu_0 = \nu_{\rm obs} \times (1 + z)$$

and

$$f_{\nu_0} = f_\nu({\rm obs})/(1 + z) .$$

The values for $\log \nu_0$ and $\log f_{\nu_0}$ are listed in Table 2. Emission-

TABLE 1

SUMMARY OF OBSERVATIONS

Object	*IUE* Image No.	Exposure Time (minutes)	Date of *IUE* Observations (UT start)	Date of Multichannel Observations
MCS 18 (0002+051)	LWR 6218	405	327.1979 21:05	360.1980
	SWP 7492	720	360.1979 18:49	
PKS 0237−233	LWR 10935	430	174.1981 06:39	262.1979
PG 0935+417	LWR 6207	570	325.1979 20:37	157.1980
Ton 1530 (1222+229)	LWR 10926	420	420.1981 06:47	158.1980
PG 1248+401	LWR 11061	365	195.1981 05:35	320.1980
	SWP 15535	411	324.1981 20:56	
PG 1522+101	LWR 13008	410	102.1982 11:04	201.1980
	SWP 17098	357	153.1982 07:06	
PG 1634+706	LWR 6477	130	361.1979 07:34	157.1980
	SWP 7216	180	328.1979 20:50	
PG 1718+481	LWR 13015	430	103.1982 10:37	159.1980
	SWP 16762	332	104.1982 10:35	
PG 2302+029	LWR 11056	410	194.1981 04:59	201.1980
	SWP 17077	297	151.1982 08:22	

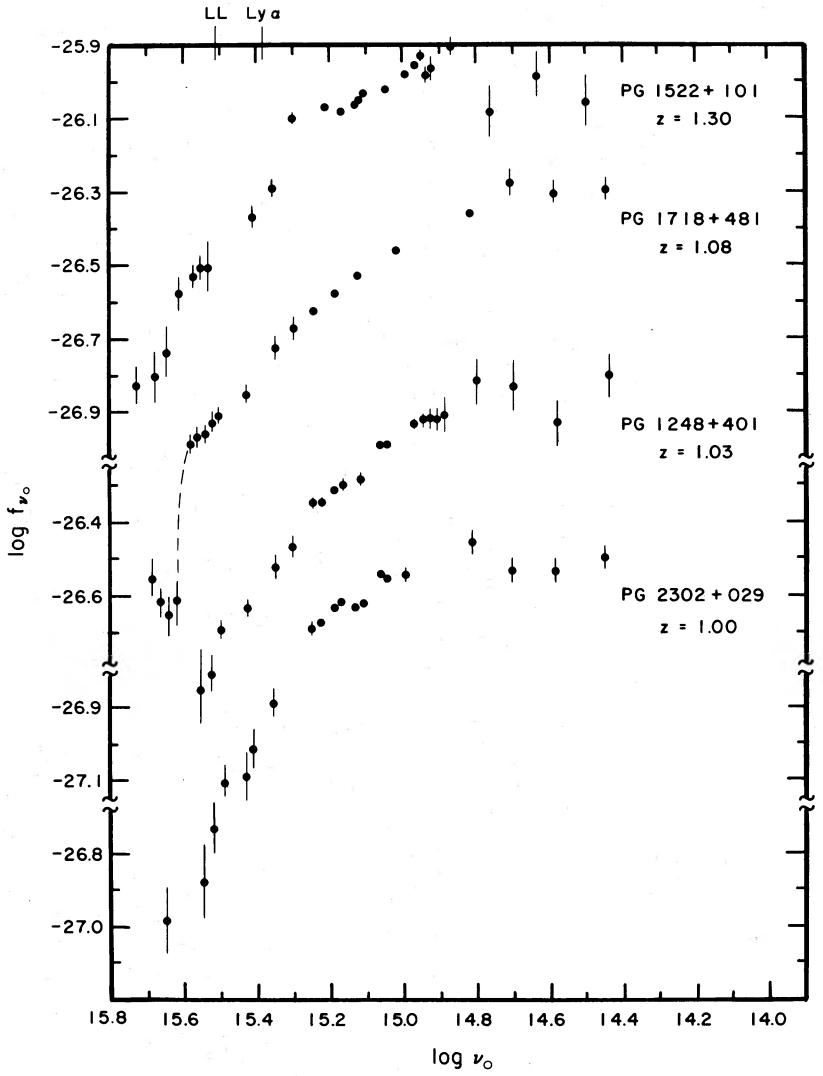

FIG. 1.—Continuum spectral energy distributions of PG 1522+101, PG 1718+481, PG 1248+401, and PG 2302+029. Log f_{ν_0}, the logarithm of the rest flux (ergs cm^{-2} s^{-1} Hz^{-1}) is plotted against log ν_0, the logarithm of the rest frequency (s^{-1}).

line redshifts are listed in Table 3 (Schmidt and Green 1983); emission-line fluxes will be discussed in a subsequent paper.

As found previously in similar studies (Green *et al.* 1980; Oke and Korycansky 1982), the continua of the five higher redshift quasars shown in Figure 2 are adequately described between Lyman-alpha and the infrared by a power law, $f_\nu \propto \nu^\alpha$ with $-0.17 \geq \alpha \geq -1.0$, whereas shortward of 1200 Å the spectral index steepens to values between -1.9 and -5.3. We have fitted two power laws to each spectrum with frequency of the break as a free parameter. The results are listed in Table 3. For Ton 1530 and PG 1634+706, the short-wavelength continuum was not consistent with a power law because of the presence of distinct Lyman discontinuities with optical depth at the Lyman limit, τ_{LL}, about 0.1. When the continua are corrected for these jumps, they yield acceptable fits to a power-law form.

By contrast, in three of the lower redshift objects, PG 1522+101, PG 1248+401, and PG 2303+029, shown in Figure 1, the continuum steepens gradually, in the sense that we are not able to find a minimum in χ^2 space corresponding to a unique frequency for a spectral index break. In the fourth object, PG 1718+481, the spectral index is constant from $\lambda_0 = 5900$ Å to $\lambda_0 = 800$ Å, where the spectrum is cut off by an optically thick Lyman limit system. For reference in the discussion below, we list in Table 3 the spectral indices for the continua shortward of Lyman-alpha and for the continua between Lyman-alpha and log $\nu_0 = 14.8$.

A number of effects can contribute to the steepening of the continua at wavelengths shortward of 1200 Å, the primary one being, as we show below, Lyman continuum absorption by intervening material. We discuss this and other causes of the continuum steepening in turn.

i) *Interstellar Reddening*

Reddening due to material in our own Galaxy can be estimated from the neutral hydrogen measurements of Heiles (1975), assuming $N_{HI}/E(B-V) = 4.8 \times 10^{21}$ atoms cm^{-2} mag^{-1} (Bohlin 1978) and applying the reddening curves of Seaton (1979). The effect of dereddening is to flatten the long-wavelength spectral index slightly, and to flatten the short-wavelength spectral index somewhat more, in some cases substantially. The spectral indices for the dereddened spectra

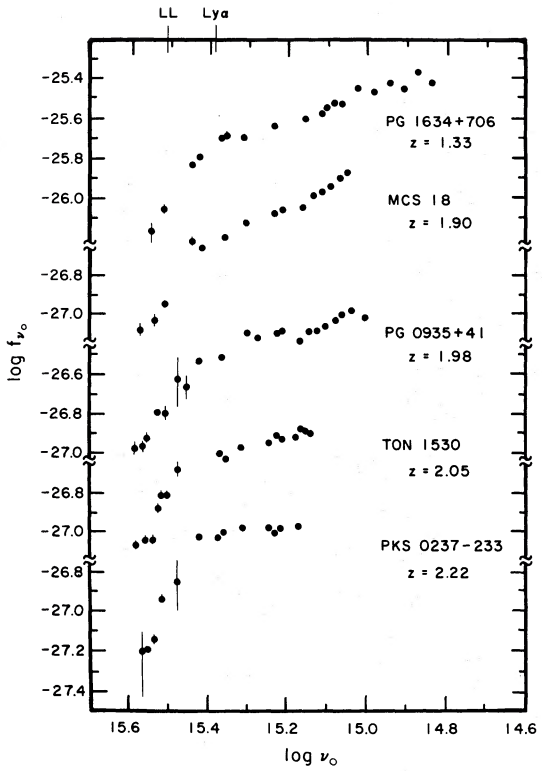

FIG. 2.—Continuum spectral energy distributions of PG 1634+706, MCS 18, PG 0935+41, Ton 1530, PKS 0237−233, as in Fig. 1.

TABLE 2

CONTINUUM FLUXES

Object	(a)	(b)	(c)	(d)
MCS 18.....	7440–7760	15.0587	−26.27	−27.64
	7120–7440	15.0774	−26.31	−27.94
	6800–7120	15.0969	−26.35	−27.67
	6480–6800	15.1174	−26.37	−27.99
	6160–6480	15.1388	−26.39	−27.80
	5780–6160	15.1635	−26.45	−27.94
	5220–5300	15.2185	−26.46	−27.72
	4980–5140	15.2354	−26.48	−27.99
	4180–4340	15.3101	−26.53	−27.55
	3700–3860	15.3620	−26.60	−28.19
	3220–3380	15.4210	−26.66	−27.68
	3096–3180	15.4429	−26.63	−28.02
	2865–2928	15.4780	−26.78	−28.30
	2600–2733	15.5136	−26.95	−28.34
	2445–2574	15.5399	−27.03	−28.21
	2157–2441	15.5700	−27.09	−28.25
	1883–1973	15.6544	−27.35	−28.26
	1798–1880	15.6749	−27.37	−28.28
	1736–1781	15.6944	−27.38	−28.25
	1670–1734	15.7086	−27.61	−27.97
	1250–1734	...	< −28.12	...
PKS 0237−233 ...	6377–6696	15.1698	−26.58	−28.78
	5789–5932	15.2174	−26.59	−28.64
	5636–5782	15.2288	−26.61	−28.77
	5481–5629	15.2407	−26.59	−28.69
	4678–4812	15.3091	−26.59	−29.02
	4212–4346	15.3540	−26.60	−29.03
	4065–4205	15.3689	−26.64	−29.07
	3604–3774	15.4185	−26.63	−28.66
	3220–3243	15.4759	−26.86	−27.33
	2904–3037	15.5130	−26.94	−28.34

TABLE 2—*Continued*

Object	(a)	(b)	(c)	(d)
	2773–2902	15.5325	−27.14	−28.51
	2641–2771	15.5531	−27.20	−28.69
	2589–2640	15.5680	−27.21	−27.28
	1880–2345	...	< −27.62	...
PG 0935+417.....	8080–8240	15.0396	−26.27	−27.10
	7600–7760	15.0660	−26.29	−27.12
	7280–7440	15.0757	−26.32	−27.34
	6960–7120	15.1038	−26.35	−27.36
	6640–6800	15.1240	−26.37	−27.70
	6320–6480	15.1452	−26.38	−27.46
	6000–6160	15.1674	−26.42	−27.75
	5380–5460	15.2173	−26.37	−27.52
	5140–5300	15.2337	−26.39	−28.02
	4700–4780	15.2756	−26.41	−27.74
	4340–4500	15.3059	−26.39	−27.90
	3700–4020	15.3645	−26.51	−28.30
	3300–3460	15.4224	−26.53	−27.51
	3140–3183	15.4514	−26.66	−27.50
	2976–2990	15.4767	−26.62	−27.11
	2728–2808	15.5092	−26.80	−27.87
	2617–2723	15.5248	−26.79	−28.55
	2507–2613	15.5413	−26.92	−28.24
	2396–2502	15.5623	−26.97	−28.18
	2272–2392	15.5836	−26.98	−28.21
	1865–2267	...	< −27.57	...
Ton 1530	6538–6670	15.1416	−26.49	−28.43
	6372–6532	15.1517	−26.48	−28.36
	6200–6366	15.1633	−26.48	−28.39
	6034–6194	15.1751	−26.51	−28.56
	5489–5614	15.2170	−26.52	−28.55
	5323–5483	15.2288	−26.50	−28.78
	5183–5317	15.2413	−26.54	−28.82
	4423–4559	15.3139	−26.57	−29.03
	3979–4112	15.3544	−26.63	−29.06
	3846–3972	15.3694	−26.60	−29.00
	3046–3069	15.4760	−26.65	−28.80
	2829–2874	15.5063	−26.80	−29.38
	2776–2829	15.5140	−26.80	−29.38
	2726–2774	15.5221	−26.88	−29.40
	2595–2726	15.5367	−27.05	−29.56
	2463–2595	15.5586	−27.05	−29.37
	2332–2463	15.5818	−27.06	−29.34
	1865–2332	...	< −27.18	...
PG 1248+401.....	7560–7800	14.8985	−26.12	−27.03
	7240–7480	14.9170	−26.13	−27.35
	6920–7160	14.9360	−26.12	−27.35
	6600–6840	14.9565	−26.13	−27.58
	6280–6520	14.9775	−26.13	−27.76
	5340–5500	15.0500	−26.19	−27.82
	5180–5340	15.0630	−26.19	−27.83
	4460–4700	15.1230	−26.29	−27.92
	4060–4140	15.1710	−26.30	−27.94
	3660–4060	15.1983	−26.32	−27.95
	3500–3660	15.2300	−26.35	−27.99
	3340–3500	15.2500	−26.35	−27.99
	2950–3050	15.3075	−26.47	−27.55
	2600–2750	15.3573	−26.52	−27.63
	2175–2375	15.4276	−26.63	−27.51
	1875–1950	15.5031	−26.69	−27.74
	1775–1875	15.5293	−26.82	−27.68
	1650–1775	15.5575	−26.86	−27.41
	1250–1650	...	< −27.37	...
PG 1522+101.....	8160–8400	14.9270	−25.99	−27.13
	7840–8160	14.9395	−26.00	−27.64
	7520–7840	14.9575	−25.95	−27.58
	7200–7520	14.9760	−25.98	−27.61
	7040–7200	14.9900	−26.00	−27.64
	6080–6240	15.0530	−26.04	−27.67

TABLE 2—*Continued*

Object	(a)	(b)	(c)	(d)
	5340–5420	15.1120	−26.06	−27.69
	5180–5340	15.1220	−26.07	−27.71
	5020–5180	15.1355	−26.09	−27.72
	4540–4700	15.1740	−26.10	−27.74
	4140–4300	15.2175	−26.09	−27.72
	3980–4140	15.2345	−26.10	−27.73
	3220–3660	15.3090	−26.13	−27.76
	2950–3125	15.3573	−26.31	−27.51
	2100–2200	15.5299	−26.53	−27.32
	1975–2075	15.5324	−26.66	−27.34
	1900–1950	15.5544	−26.54	−27.65
	1775–1900	15.5776	−26.56	−27.74
	1650–1775	15.6084	−26.61	−27.56
	1525–1650	15.6416	−26.76	−27.55
	1400–1525	15.6775	−26.83	−27.56
	1250–1400	15.7209	−26.85	−27.69
PG 1634+706.....	9840–10320	14.8418	−25.52	−26.63
	9040–9680	14.8740	−25.48	−26.78
	8400–8800	14.9107	−25.55	−26.89
	7600–8240	14.9465	−25.52	−27.40
	6960–7440	14.9879	−25.56	−27.77
	6320–6800	15.0283	−25.55	−27.88
	5840–6160	15.0671	−25.62	−27.74
	5620–5780	15.0894	−25.62	−27.43
	5380–5540	15.1080	−25.65	−27.45
	5060–5300	15.1309	−25.69	−27.72
	4740–4980	15.1586	−25.71	−27.74
	4020–4180	15.2324	−25.75	−27.68
	3300–3540	15.3100	−25.79	−27.24
	3047–3149	15.3541	−25.79	−27.22
	2941–3047	15.3693	−25.81	−27.63
	2617–2733	15.4278	−25.90	−27.81
	2494–2617	15.4381	−25.94	−27.88
	2330–2347	15.4760	−25.94	−26.42
	2064–2197	15.5167	−26.16	−27.50
	1919–2059	15.5466	−26.27	−27.39
	1880–1919	15.5666	−26.32	−27.59
	1821–1856	15.5808	−26.87	−27.59
	1250–1808	...	< −27.83	...
PG 1718+481.....	8260–10420	14.8250	−25.55	−26.88
	5460–6380	15.0259	−25.65	−27.29
	4500–4820	15.1275	−25.73	−27.36
	3700–4240	15.1938	−25.78	−27.41
	3220–3700	15.2471	−25.82	−27.46
	3025–3150	15.3060	−25.88	−26.97
	2700–2825	15.3539	−25.92	−27.04
	2250–2450	15.4290	−26.05	−27.39
	1900–1965	15.5108	−26.12	−27.51
	1825–1900	15.5280	−26.13	−27.46
	1750–1825	15.5460	−26.16	−27.36
	1675–1750	15.5647	−26.18	−27.40
	1600–1675	15.5843	−26.19	−27.39
	1475–1550	15.6191	−26.62	−27.42
	1400–1475	15.6414	−26.66	−27.46
	1325–1400	15.6648	−26.62	−27.59
	1250–1325	15.6879	−26.56	−27.45
PG 2303+029.....	6240–6440	14.9870	−26.04	−27.19
	5460–5550	15.0470	−26.06	−27.39
	5380–5460	15.0442	−26.04	−27.37
	5300–5380	15.0506	−26.04	−27.37
	4660–4740	15.1061	−26.11	−27.74
	4500–4580	15.1211	−26.15	−27.48
	4420–4500	15.1288	−26.13	−27.45
	4100–4180	15.1612	−26.12	−27.75
	3900–4100	15.1761	−26.14	−27.47
	3700–3900	15.1984	−26.13	−26.51
	3620–3700	15.2147	−26.18	−27.33
	3540–3620	15.2243	−26.16	−27.49
	3460–3540	15.2341	−26.18	−27.32
	3380–3460	15.2441	−26.19	−27.34

TABLE 2—*Continued*

Object	(a)	(b)	(c)	(d)
	2900–3000	15.3083	−26.33	−27.57
	2575–2700	15.3570	−26.39	−27.59
	2225–2350	15.4188	−26.52	−27.44
	2150–2225	15.4352	−26.60	−27.29
	1850–1950	15.4994	−26.61	−27.61
	1725–1850	15.5259	−26.74	−27.51
	1625–1725	15.5541	−26.88	−27.45
	1250–1350	15.6642	−26.98	−27.64

(a) Observed wavelength interval (Å), used to find average f_{ν_0}.
(b) Logarithm of rest frequency (s^{-1}) corresponding to central wavelength of interval given in (a).
(c) Logarithm of the rest frame, f_{ν_0}, in ergs cm^{-2} s^{-1} Hz^{-1}. Three sigma upper limits are given when no net flux observed.
(d) Logarithm of the mean error in the rest flux, as in (c).

TABLE 3

SPECTRAL INDICES

Object	(a)	(b)	(c)	(d)	(e)	(f)
MCS 18	1.90	0.08	0.03	1.01	3.27	1115
				0.85	2.81	
				0.71	0.45	
PKS 0237−233	2.22	0.02	0.03	0.17	5.34	1119
				0.17	4.96	
				0.09	4.70	
PG 0935+417	1.98	0.04	0.04	0.26	1.93	1222
				0.19	1.72	
				0.13	0.79	
Ton 1530	2.05	0.08	0.01	0.56	3.49	1017
				0.44	2.79	
				0.25	1.47	
PG 1248+401	1.03	0.04	0.05	0.18	1.76	1216[g]
				0.13	1.67	
				0.017	0.66	
PG 1522+101	1.30	0.08	0.02	0.40	1.44	1216[g]
				0.26	1.26	
				0.17	0.28	
PG 1634+706	1.33	0.06	0.05	0.85	2.10	1469
				0.76	1.65	
				0.40	0.62	
PG 1718+481	1.08	0.03	0.01	0.33	1.04	3000[g]
				0.30	0.92	
				0.09	0.77	
PG 2302+029	1.00	0.10	0.05	0.31	1.96	1216[g]
				0.19	0.61	
				0.06	0.53	

(a) Emission-line redshift, from Schmidt and Green 1983.
(b) Galactic $E(B-V)$ (see text).
(c) Upper limit to intrinsic $E(B-V)$ (see text).
(d) Spectral index α_1, for $f_\nu \propto \nu^\alpha$, $\lambda > \lambda_B$; first line, no reddening correction; second line, corrected for Galactic reddening; third line, corrected for Galactic and intrinsic reddening.
(e) Spectral index α_2, for $\lambda < \lambda_B$; as in (b).
(f) Wavelength of spectral index break, λ_B.
(g) Wavelength of spectral index break was chosen arbitrarily (see text).

are listed in Table 3. In all cases, however, the spectra still steepen significantly shortward of 1200 Å in the quasar frame.

ii) *Absorption by Intervening Material*

Oke and Korycansky (1982) have discussed the steepening of the continua shortward of redshifted 1216 Å in a sample of high-redshift quasars in terms of Lyman continuum absorption by intervening material, unrelated to the quasar. In this picture, the quasar continuum between Lyman-alpha and Lyman-beta is depressed by Lyman-alpha absorption lines; between Lyman-beta and the Lyman limit it is depressed by Lyman-beta and higher order Lyman lines, primarily Lyman-beta; and shortward of 912 Å, by Lyman continuum absorption arising from clouds of moderate optical depths.

We find strong evidence for this interpretation. In Figure 3*a* we have plotted $\Delta\alpha$, the change in spectral index at 1200 Å, as a function of $\log(1 + z_{em})$, and in Figure 3*b* as a function of $\log L$, where

$$\log L = \log f_{\nu_{2500\,\text{Å}}} + \log\left(z + \frac{1}{2}z^2\right)^2 + \log\frac{4\pi c^2}{H_0{}^2}$$

(Richstone and Schmidt 1980), is the luminosity of the quasar at 2500 Å, for a Friedmann universe with $q_0 = 0$ and $\Lambda = 0$ and $H_0 = 50$ km s^{-1} Mpc^{-1}. Included are the data from this paper, from *IUE* observations by Green *et al.* (1980), and from the very high-redshift sample of Oke and Korycansky (1982). We have used the spectral indices derived without correction for Galactic reddening, in order to make a direct comparison with the published Oke and Korycansky data, but the effect of Galactic reddening on $\Delta\alpha$ is negligible.

The change in spectral index, $\Delta\alpha$, is uncorrelated with $\log L$ but is correlated with $\log(1 + z_{em})$ at the five sigma level. The most straightforward interpretation is that the steepening is primarily caused by intervening absorption and is not a function of an intrinsic property of the quasar. It is possible that the steepening is intrinsic and is a function of redshift because of evolution in some intrinsic quasar property which is somehow unrelated to quasar luminosity, but we find this unlikely. The slope above 1200 Å is not correlated with either $\log L$ or $\log(1 + z_{em})$, in accordance with other studies (Richstone and Schmidt 1980).

The viability of this interpretation is directly testable in the objects for which higher resolution spectra of the narrow Lyman-alpha absorption lines are available from the ground. These data suggest that the steepening of the continuum slope shortward of 1200 Å in data of low spectral resolution and low signal-to-noise ratio is in fact due to the composite effect of the Lyman continuum absorption associated with the highest column density Lyman-alpha systems. For two of our high-redshift objects, PG 0935+410 and Ton 1530, we have obtained 1.5 Å resolution spectra at the Steward Observatory 90 inch shortward of Lyman-alpha in emission (Figs. 4*a* and 4*b*), and for a third, PKS 0237−233, observations of Lyman-alpha were taken from Boroson *et al.* (1978). Line centers and equivalent widths for the observed absorption features in PG 0935+410 and Ton 1530 are listed in Table 4. For an observed Lyman-alpha line with measured equivalent width, given a value of the Doppler parameter b, we can calculate the resulting optical depth at the Lyman limit, τ_{LL}, from the Lyman curve of growth (Chaffee 1982). In some cases we can measure τ_{LL} for an individual system and directly derive b (see Table 6). In other cases, the lack of observable discrete Lyman edges sets an upper limit to τ_{LL} of about 0.2, and hence a lower limit to b. Weak Lyman-alpha lines with $W_{\lambda_0} < 0.5$ Å are optically thin for any plausible value of b, but for lines with $W_{\lambda_0} > 0.5$ Å, we find that $b \approx 20$–30 km s^{-1} is required. An upper limit to b can be derived by requiring that the summed effect of the Lyman edges is consistent with the requirement that the corrections to the flux bring the continuum back up to the

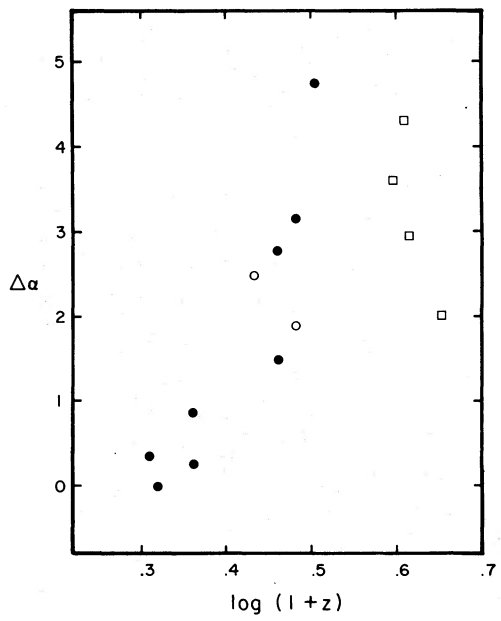

FIG. 3*a*

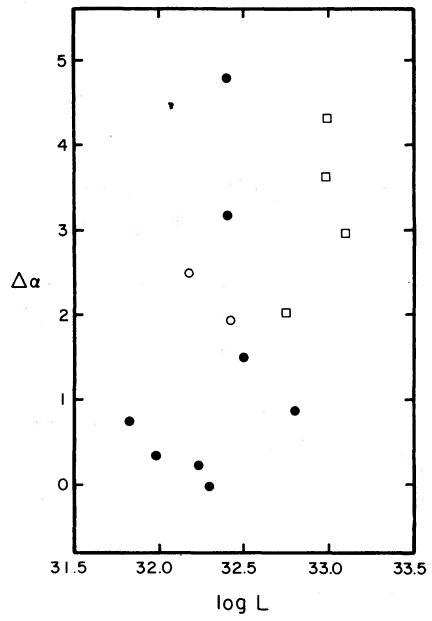

FIG. 3*b*

FIG. 3.—(*a*) Change in spectral index, $\Delta\alpha$, plotted against $\log(1 + z_{em})$. Open boxes are data from Oke and Korycansky (1982); open circles are from Green *et al.* (1980); and closed circles are from this work. (*b*) Change in spectral index, $\Delta\alpha$, plotted against $\log L$, the luminosity of the quasar at 2500 Å. Symbols are as in Fig. 3*a*.

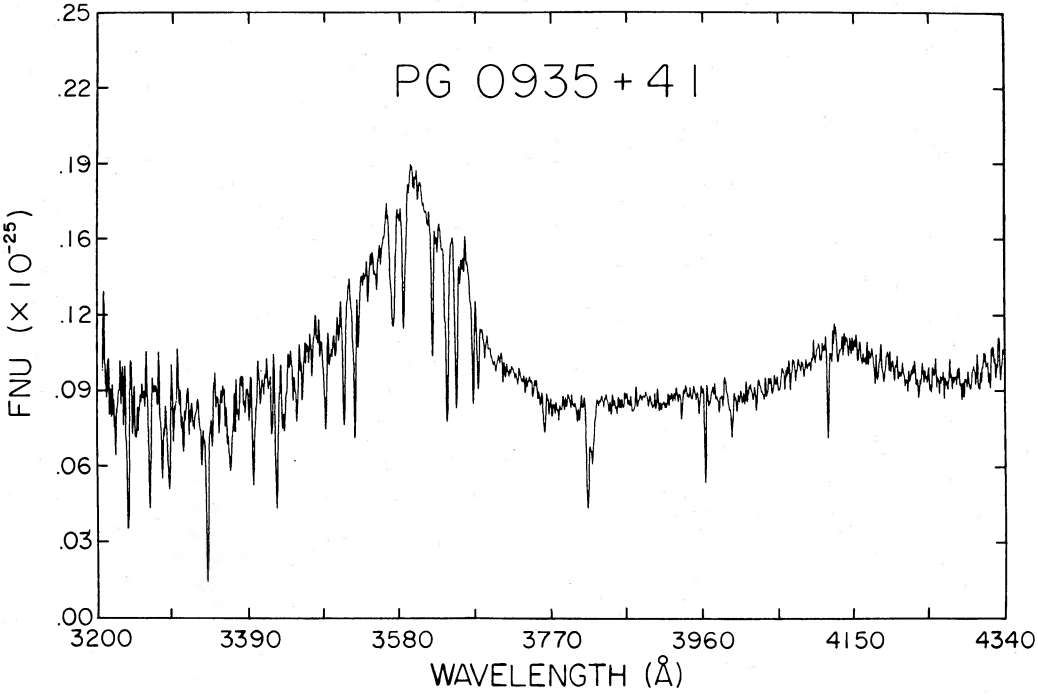

FIG. 4*a*

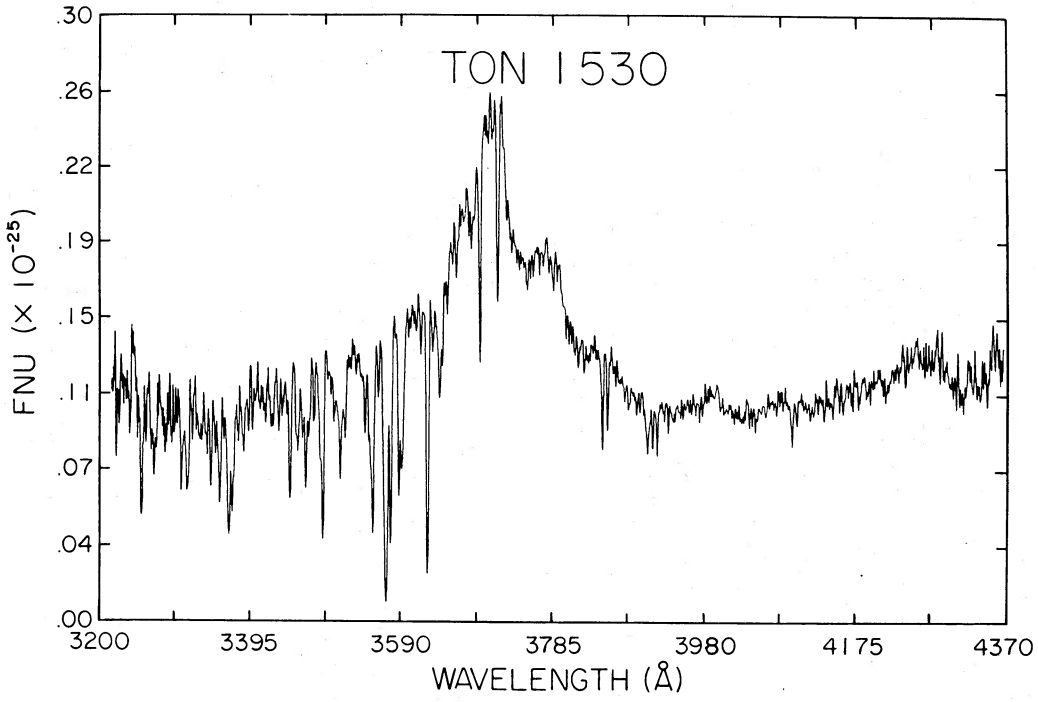

FIG 4*b*

FIG. 4.—(*a*) Spectrum of PG 0935+410 obtained with the Steward Observatory 90 inch telescope, Boller & Chivens spectrograph, and blue pulse-counting Reticon detector. (*b*) Spectrum of Ton 1530, also obtained with the Steward Observatory 90 inch telescope, Boller & Chivens spectrograph, and blue pulse-counting Reticon detector.

TABLE 4

ABSORPTION-LINE LISTS

Line No.	Line Center[a]	W[b]	Line ID	b[c]	τ_{LL}[d]
Ton 1530:					
1	3254.3	1.98	...	...	...
2	3271.0	...	...	...	...
3	3306.1	1.17	...	...	...
4	3314.0	1.87	...	...	...
5	3355.5	1.71	...	...	...
6	3367.6	4.60	blend with 7	40	0.02
7	3372.0	...	...	...	...
8	3446.2	1.33	...	35	0.10
9	3466.3	1.52	...	35	0.15
10	3488.6	2.68	...	40	0.007
11	3511.1	1.99	...	39	0.06
12	3553.0	3.66	...	60	0.00
13	3570.1	5.55	C IV (1548)	...	...
14	3575.9	2.34	C IV (1550)	...	...
15	3586.9	0.74	...	35	0.002
16	3590.5	2.71	...	40	0.006
17	3623.1	3.62	...	39	0.24
18	3639.3	2.22	...	39	0.08
19	3691.4	3.03	...	40	0.007
20	3713.7	1.19	...	...	...
21	3848.9	0.99	C IV (1548)	...	...
22	3855.7	0.58	C IV (1550)	...	...
23	3906.9	0.91	C IV (1548)	...	...
24	3913.7	0.34	C IV (1550)	...	...
25	3919.1	0.40	...	...	...
26	4093.2	0.45	...	...	...
PG 0935+417:					
1	3224.1	1.04	...	35	0.06
2	3239.4	1.93	...	40	0.004
3	3266.1	1.44	...	40	0.002
4	3282.2	1.46	...	40	0.002
5	3290.7	1.65	...	40	0.003
6	3309.3	1.18	...	35	0.08
7	3338.2	3.58	...	39	0.28
8	3367.9	2.68	...	39	0.14
9	3396.3	1.17	...	35	0.07
10	3425.4	1.72	...	40	0.003
11	3434.3	1.08	...	35	0.05
12	3450.4	1.26	...	35	0.02
13	3487.3	1.10	...	35	0.05
14	3510.2	1.16	...	35	0.06
15	3524.2	1.72	...	35	0.20
16	3572.5	2.24	...	38	0.16
17	3585.1	1.98	...	38	0.11
18	3621.6	0.84	...	...	...
19	3639.6	1.99	...	...	...
20	3651.1	1.40	...	...	...
21	3672.3	0.84	C IV (1548)	...	...
22	3678.0	0.59	C IV (1550)	...	...
23	3761.9	0.41	...	...	...
24	3815.9	1.74	C IV (1548)	...	...
25	3821.8	1.36	C IV (1550)	...	...
26	3933.5	0.18	...	...	...
27	3963.3	0.71	...	...	...
28	3996.5	0.53	...	...	...
29	4117.2	0.96	...	...	...

[a] Observed wavelength of centroid of line.
[b] Observed equivalent width (Å).
[c] Assumed model b-values, km s^{-1} (see text).
[d] Assumed model τ_{LL} (see text).

extrapolation of the optical power law, which we have corrected for Galactic reddening only. We find that in every case, a handful of absorbers, about four to eight, with $20 \leq b \leq 50$ km s^{-1} and $\tau_{LL} \approx 0.08$ is adequate. Implied values of b and τ_{LL} corresponding to specific Lyman-alpha absorption lines are listed in Table 4, for one reasonable model; other models are possible. A prediction of this explanation of the continuum steepening is that high signal-to-noise observations of the continuum shortward of 912 Å should reveal a small number of discrete, optically thin Lyman edges, with $\tau_{LL} \approx 0.1$.

If the steepening is caused by four to eight absorbers along the line of sight to the higher z objects, and if the comoving density of absorbers is constant, then one would expect that two to four absorbers would be responsible for the steepening in the low-redshift objects. This is consistent with the observation that out of five objects with $z \leq 1.33$, one object, PG 1718+481, shows no steepening beyond 912 Å, implying that its line of sight does not pass through any $\tau \approx 0.1$ Lyman limit absorber, until the $\tau = 1$ Lyman discontinuity listed in Table 6.

It is of interest to ask whether these absorbers can be identified with the metal-poor Lyman-alpha "forest" clouds or with the metal-containing galactic halo absorbers. Direct detection of associated C IV or Mg II absorption is not feasible, since the column densities of these systems are so low that for reasonable ionization levels and solar abundances, the metal lines should have equivalent widths at only the milliangstrom level. Recently, Carswell *et al.* (1984) have found evidence that suggests that the Lyman-alpha forest population of absorbers cannot in general be responsible for the UV spectral steepening we observe in QSOs. They have observed the Lyman-alpha forest in one object at $z_{em} = 2.01$, Q1101−264, at 20 km s^{-1} resolution. By Voigt fitting of the line profiles they derive column densities directly. In this object, three clouds identified at lower resolution by Young, Sargent, and Boksenberg (1982*b*), with equivalent widths greater than 0.5 Å, were resolved into several, much weaker components by Carswell *et al.* In fact, Carswell *et al.* observe no system with $N(\text{H I}) \geq 10^{15}$ cm^{-2}, and the accumulated effect of all the absorbers they see would be completely negligible at the Lyman limit. Unfortunately, *IUE* observations of this QSO by Boksenberg and Snijders (1981) do not give much information about the continuum shape past 912 Å in the QSOs frame since the spectrum is cut off at $z = 1.8$ by an optically thick, metal-containing Lyman limit system. If only very low column densities for Lyman-alpha forest clouds continue to be found when more observations become available, then the effect of the Lyman-alpha forest on the spectral steepening shortward of the Lyman limit is negligible. It is possible that a very high column density tail to the Lyman-alpha forest population has been found (see Robertson, Shaver, and Carswell 1983 and Roser *et al.* 1983 for examples), but these systems are probably so rare that they cannot be responsible in general for the steepening which is seen commonly in high-z QSOs.

Instead, we hypothesize that the absorbers responsible for the steepening are the low column density tail of the distribution of metal-containing, galactic halo systems. We see examples of systems with τ_{LL} as low as 0.3 (see Table 6), and it is plausible that they exist at $\tau_{LL} \approx 0.1$. While the implication is that galactic halos have to be uncomfortably large for our line of sight to intersect them so often (see discussion below), the alternative is a correlation between intrinsic quasar properties and z, which is even more difficult to explain.

The continuum between emission Lyman-alpha and the Lyman limit in the lower redshift objects can also yield information about the nature of the Lyman-alpha absorbers at redshifts lower than those for which high-resolution spectra are currently available. In order to compare our data at low

redshifts with the Oke and Korycansky high-redshift data, we have computed

$$D_A = \left\langle 1 - \frac{f_\nu(\text{obs})}{f_\nu(\text{cont})} \right\rangle$$

between Lyman-alpha and Lyman-beta, and D_B, the analogous quantity between Lyman-beta and the Lyman limit, where f_ν(obs) is the observed continuum level, and f_ν(cont) is the continuum level obtained by extrapolating the continuum on the long-wavelength side of Lyman-alpha. In the discussion which follows, we use quantities derived for the spectra with no correction for interstellar reddening. In Table 5, we list $\langle D_A \rangle$ and $\langle D_B \rangle$ for the spectra with reddening corrections, and it is clear that the effect is negligible. The quantity $\langle D_A \rangle$ is proportional to the total equivalent width of Lyman absorption, or

$$\langle D_A \rangle \propto \sum_i \frac{dN_i}{dz} \Delta z W_i ,$$

where dN_i/dz is the number of absorbers per redshift of a given equivalent width, W_i, and Δz is the observed redshift interval, and the sum is over all equivalent widths. If the spectrum of equivalent widths is constant with z, but only the total number density changes as $dN/dz \propto (1+z)^\gamma$, then $\langle D_A \rangle \propto (1+z)^\gamma$. For no evolution in the comoving density of absorbers and $q_0 = 0$, $\gamma = 1$. In Table 5 we list the values for $\langle D_A \rangle$, $\langle D_B \rangle$, and $\langle D_B/D_A \rangle$ for the lower redshift quasars in our sample (PG 1718+481, PG 2303+029, PG 1634+706, PG 1248+401, and PG 1522+101), the intermediate-redshift QSOs observed with *IUE* (PKS 0237−233, Ton 1530, PG 0935+417, and PG 1115+080), and the Oke and Korycansky high-redshift sample. We derive $\gamma = 1.29 \pm 0.21$ for z between 1.0 and 3.5, which is consistent with no evolution of the distribution of absorbers with redshift. By comparison, in the high-resolution studies of QSOs with $z > 1.6$ which explicitly count lines that have $W_{\lambda_0} > 0.32$ Å, Sargent *et al.* (1980) find $\gamma = 1.6 \pm 1.3$, Young, Sargent, and Boksenberg (1982*a*) find $\gamma = 1.8 \pm 0.5$, and convincing evidence for a steep $\gamma = 2.2 \pm 0.4$ is found by Peterson (1983). Very steep evolution of the number density toward low redshifts is inconsistent with our data, unless the equivalent width spectrum of absorbers changes in an appropriate way. It is also possible that intrinsic steepening of the continuum or a trace of intrinsic reddening may be dominating the steepening in this restricted wavelength region.

To investigate the possibility that the equivalent width spectrum changes, one might hope to study the evolution of the average thermal width of the Lyman clouds, $b = (kT/m)^{1/2}$, which can be estimated by $\langle D_B/D_A \rangle$ (see Oke and Korycansky 1982). Unfortunately, $\langle D_B/D_A \rangle$ is not very sensitive to the expected changes in b. In the models of Ostriker and Ikeuchi (1983), for example, b decreases by 25% between $z = 3.5$ and $z = 1.0$, corresponding to $\Delta\langle D_B/D_A \rangle \approx 0.1$, which we would not be able to detect.

TABLE 5

BROAD-BAND LYMAN-ALPHA ABSORPTION

Parameter	Oke and Korycansky	*IUE* High-z	*IUE* Low-z
$\langle z_{em} \rangle$	2.977	2.04	1.14
$\langle z_{abs} \rangle$	2.75	1.87	1.02
Δz_A	0.32	0.25	0.17
Δz_B	0.13	0.098	0.069
$\langle D_A \rangle$	0.29 ± 0.02	0.19 ± 0.10	0.13 ± 0.04
$\langle D_B \rangle$	0.39 ± 0.02	0.45 ± 0.22	0.11 ± 0.05
$\langle D_B/D_A \rangle$	1.40 ± 0.06	2.28 ± 0.86	0.81 ± 0.23
Dereddened:			
$\langle D_A \rangle$	...	0.19 ± 0.11	0.13 ± 0.05
$\langle D_B \rangle$	...	0.45 ± 0.23	0.14 ± 0.04
$\langle D_B/D_A \rangle$ ...	...	2.51 ± 0.57	1.43 ± 0.36

iii) *Reddening Internal to the QSO and along the Line of Sight*

As shown above, reddening by dust in the immediate vicinity of the quasar cannot be the major source of spectral steepening shortward of 1200 Å, unless the dust content of quasars is a function of redshift and not luminosity, which is unlikely. However, two of the low-redshift objects, PG 1248+401 and PG 2302+029, show gentle curvature longward of 1200 Å, where obviously, Lyman-alpha or Lyman continuum absorption cannot be the cause of a deviation from a power law.

Although the form of the reddening curve in QSOs is completely unknown, if we apply the Milky Way curve to deredden these two objects, the result can be made consistent with a power law, for $E(B-V) = 0.05$, intrinsic to the quasar, a value that is typical for a high-latitude line of sight in our Galaxy. However, we note that in none of our objects do we see a Lyman discontinuity at the emission-line redshift, so that $N(\text{H I}) \leq 2 \times 10^{17}$ cm^{-2}, and if $N(\text{H I})/E(B-V) = 4.8 \times 10^{21}$ atoms cm^{-2} mag^{-1}, then $E(B-V) \leq 4 \times 10^{-5}$. Thus, reddening intrinsic to the quasar, although potentially important, is probably negligible, unless the dust to neutral gas ratio in these objects is peculiarly high.

An identical argument applies to the dust content of the $\tau_{LL} \approx 0.1$ clouds postulated to produce the quasar spectral slope steepening through Lyman continuum absorption. Similarly, dust in the optically thick $\tau_{LL} \geq 1.0$ Lyman limit systems, discussed in § III*b*, has no effect unless $\tau_{LL} \gg 10$. While our line of sight no doubt passes through a $\tau_{LL} > 10$ system occasionally, such a thick system is probably rare (see § III*b* and the H I observations of Briggs 1982 for a discussion of this point), so that most of these systems have $\tau_{LL} < 10$. Thus reddening associated with galaxies along the line of sight is generally negligible and cannot cause continuum steepening in the majority of QSOs.

Recently, it has been suggested that intergalactic space might be uniformly filled with dust as a by-product of violent galaxy formation (Ostriker and Cowie 1981; Ostriker and Heisler 1984). This dust would then cause spectral steepening in QSOs, with an increase in steepening at higher redshifts. In order to obtain a significant *dust* opacity, however, these authors must assume an ambient intergalactic *total* hydrogen density that is five orders of magnitude larger than the upper limit to the diffuse *neutral* hydrogen density derived from Gunn-Peterson tests at Lyman-alpha (Gunn and Peterson 1965). Thus we must again invoke a very peculiar neutral hydrogen to dust ratio to explain the continuum steepening in terms of intergalactic reddening. Lacking direct observations of intergalactic dust, we prefer the simpler explanation of Lyman continuum absorption described above.

iv) *Intrinsic Steepening of the QSO Continuum*

Since the extrapolation of the optical continuum above Lyman-alpha to very short wavelengths greatly overestimates the observed X-ray flux in many QSOs (Tananbaum *et al.* 1979; Zamorani *et al.* 1981), it is clear that the continuum must steepen somewhere in the extreme-UV. In two of the objects in our sample (PG 1634+706 and Ton 1530) and one

presented by Green *et al.* (1980) (PG 1115+080), the extrapolation of the observed continuum slope shortward of Lyman-alpha underestimates the X-ray fluxes as measured by the *Einstein Observatory* Imaging Proportional Counter (IPC), implying that the continuum must once again flatten out in the extreme-UV of these objects. Determining the exact form of the energy distribution is important to the understanding of the physical processes that give rise to the optical/UV continuum.

Several authors have discussed models in which the bulk of the optical/UV continuum arises from thermal emission from an accretion disk (Lynden-Bell 1969; Shields 1978), and Malkan and Sargent (1982) have suggested that the UV spectral steepening should take the form of the Wien side of a blackbody at the temperature of the hottest thermal component, or a somewhat broader shape, when more realistic models for optically thick accretion disks are considered (Malkan 1983). As argued above, the corrections for intervening absorption and reddening are sufficiently uncertain that detailed modeling of the intrinsic quasar continuum does not provide strong constraints on accretion disk parameters. If, however, the UV/optical continuum represents thermal emission, the hottest thermal component of which falls off shortward of our data, then the implied temperatures are hotter than about 55,000 K. An upper limit to the hottest temperature is about 3×10^5 K, derived by requiring that the exponential fall through the X-ray flux points in PG 1634+706 and Ton 1530.

An alternative emission mechanism for the optical/UV continuum is nonthermal synchrotron self-Compton (SSC) discussed by Jones, O'Dell, and Stein (1974*a*, *b*). Puetter *et al.* (1982) model the shape of the blue continuum for QSOs with a combination of SSC emission and optically thick Balmer continuum emission. In the SSC picture, the UV spectral steepening results from inverse Compton energy losses suffered by the high-energy electrons and is a function of the magnetic field strength, source geometry, and particle injection mechanisms. By invoking multiple synchrotron components and continuous injection of high-energy particles, one can fit the observed optical/UV continuum with reasonable source parameters (e.g., Puetter *et al.* 1982). A test of this interpretation would be a measurement of the associated inverse Compton radiation at X-ray and γ-ray energies. The spectrum of this radiation should have a power-law spectral index similar to the optical power-law index, and a cutoff at $\nu = 10^{21}$ Hz, if the steepening of the spectral index we observe at $\nu = 10^{15.5}$ Hz is caused by a synchrotron cutoff, although other sources of a γ-ray cutoff are possible (e.g., Dean and Ramsden 1981, and references therein).

In principle, the intrinsic ultraviolet spectrum seen by the broad emission-line material in the quasar can be deduced through modeling of the line-emitting gas. If the observed UV spectrum appears steeper than the spectrum implied by broad-line fluxes, then this may indicate reddening by dust or absorption by gas between us and the broad-line region (Shuder and MacAlpine 1979; Netzer and Davidson 1979). Optically thin lines produced predominantly by recombination are the most straightforward to interpret in this regard. MacAlpine (1981) has claimed that if the intrinsic continuum were to steepen shortward of Lyman-alpha as sharply as is observed in many high-redshift objects, then there would not be enough UV flux to produce the observed equivalent width of He II λ4686, provided that this line is produced by recombination and radiative cascading. However, He II λ1640 is expected to be 5–10 times as strong as λ4686, and so should have an equivalent width of 150–300 Å for MacAlpine's argument to be valid; and λ1640 is not observed at this level in these high-luminosity objects, with an upper limit of a few angstroms for PG 1115+080 (Young *et al.* 1982*a*). In addition, He II λ4686 may be enhanced by pumping of the He II (2–4) transition by hydrogen Lyman-alpha (MacAlpine 1981), and uncertainties in estimating this effect are sufficiently large that precise conclusions about the UV continuum are difficult to make (Grandi 1983). Essentially all other lines commonly seen in QSO spectra are strongly affected by line trapping, fluorescent processes, collisional de-excitation, or conditions in the X-ray heated warm zone behind the Strömgren sphere (Davidson and Netzer 1979, and references therein; Kwan and Krolik 1981; Canfield and Puetter 1980, 1981; Ferland and Netzer 1979; Mathews, Blumenthal, and Grandi 1980; Weisheit, Shields, and Tarter 1981). Lines that may not be primarily produced in this zone (e.g., Lyman-alpha, C IV, C III]) may be most sensitive to the UV continuum spectral shape since they are more or less independent of the spectrum and intensity of the X-ray flux (Mushotzky and Ferland 1984), but such interpretations are probably complicated by uncertainties in the geometry and distribution of the broad-line clouds. At least one modern broad-line region calculation requires spectral indices between the Lyman limit and the softest X-rays, $\alpha > -2$, to reproduce the observed line ratios (Kwan and Krolik 1981). This is further evidence that suggests that reddening or absorption has indeed modified the observed spectrum we see.

Eastman, MacAlpine, and Richstone (1983) have pursued a model in which the spectral steepening is caused by Lyman-alpha absorption by cloudlets associated with the QSO but outside the broad-line region. This model postulates a near continuum of absorption by a multitude of optically thin cloudlets. By construction, it successfully fits the observed spectrum of PG 1115+080, detected down to a rest wavelength of 432 Å by Green *et al.* (1980). (We note that we can fit the spectral energy distribution in that object by correcting for Galactic reddening and approximately 10 optically thin Lyman continuum absorbers.) Major objections to the Eastman *et al.* model are the ad hoc velocity distribution of the absorbers and the unrealistically large amounts of kinetic energy stored in the cloudlets.

In summary, we have argued that the observed steepening of the continua shortward of 1200 Å arises primarily from Lyman continuum absorption by intervening material. Reddening intrinsic to the quasar and along the line of sight could contribute but is probably a small effect, as is Galactic reddening. Intrinsic steepening cannot be strictly ruled out in any particular object and is perhaps apparent in the spectra of PG 1248+401 and PG 2302+029. However, it is difficult to describe quantitatively how the intrinsic spectrum steepens, because of uncertainties in the corrections for absorption and reddening.

b) The Lyman Limit Discontinuities

The continua in six of our objects are cut off by an optically thick Lyman limit system with redshift $z_{LL} \ll z_{em}$. In addition, three other Lyman discontinuities are seen with optical depth $\tau_{LL} \approx 1.0$. Table 6 lists the redshifts of these systems, values for, or limits to, τ_{LL}, and equivalent widths for the associated Lyman-alpha line when available. We have investigated the nature of these absorption systems by studying their statistical

TABLE 6

LYMAN LIMIT SYSTEMS

Object	(a)	(b)	(c)	(d)	(e)	(f)	(g)	(h)	(i)	(j)
PG 1248+401	1600 ± 25	0.773	2.23	3.54(17)	...	Mg II	4956.8	0.887	3.3(13)	20
							4969.2	0.662		
PG 1718+481	1559 ± 1	0.713	0.99	1.57(17)	2.8 ± 1.0	Mg II	(4785)	<0.05	...	...
PG 1634+706	1867 ± 4	1.046	1.19	1.89(17)	...	Mg II	5721.8	0.140	...	...
							5706.9	0.100		
	1818 ± 4	0.993	2.18	3.46(17)	...	Mg II	5563.8	1.20	...	...
							5578.1	0.78		
MCS 18	1690 ± 20	0.850	1.69	2.68(17)	...	Mg II	5177.1	1.270	3.2(13)	35
							5188.2	0.857		
PG 0935+417	2267 ± 4	1.464	1.39	2.21(17)	...	C IV	3815.9	1.74	5.5(14)	48
							3821.8	1.36		
	...	1.372	...	...	6.8 ± 3	C IV	3672.3	0.84	1.9(14)	29
							3678.0	0.59		
Ton 1530	2720 ± 2	1.98	0.30	4.76(16)	1.22[k]	C IV	4612.8	1.3[k]	6.5(13)	51
							4620.5	0.5[k]		
	2257 ± 10	1.486	1.27	2.02(17)	...	C IV	3848.9	0.99	1.4(14)	56
							3855.7	0.58		
PKS 0237−233	2350 ± 10	1.560	0.75	1.19(17)	...	C IV	3963.7	0.2[l]	2.0(13)	...
							3970.6	0.1[l]		

(a) Observed wavelength of Lyman discontinuity (Å).
(b) Redshift computed from observed metal-line wavelength if available; otherwise, from Lyman limit wavelength.
(c) Optical depth at the Lyman limit, τ_{LL}.
(d) Column density of neutral hydrogen, derived from τ_{LL} (cm^{-2}).
(e) Observed equivalent width of Lyman-alpha (Å).
(f) Metal species observed.
(g) Observed wavelength of doublets (Å).
(h) Observed equivalent widths of doublets (Å).
(i) Column density of metal species (cm^{-2}).
(j) Doppler width of metal species (km s^{-1}).
(k) Morton and Morton 1972.
(l) Boroson *et al.* 1978.

distribution and by searching for associated C IV and Mg II absorption lines from the ground.

i) *Statistical Distribution*

Optically thick Lyman limit discontinuities are observable in low-resolution spectra, and a large body of observational material is available to study their distribution over a wide range of redshift. Surveys of very high redshift quasars from the ground (Smith *et al.* 1981; Oke and Korycansky 1982; MacAlpine and Feldman 1982) can be combined with the data of this paper and other *IUE* data (Green *et al.* 1980; Snijders 1980; Elvis and Fabbiano 1982) to assemble a sample of 35 Lyman limit systems between $z = 0.4$ and $z = 3.5$ along 72 QSO lines of sight. A subset of this sample is discussed by Tytler (1982).

We arbitrarily divide the Lyman limit systems (LLSs) into two groups: those with "ejection" velocity with respect to the quasar emission redshift $\beta > 0.02$, and those with $\beta \leq 0.02$, where

$$\beta = \frac{R^2 - 1}{R^2 + 1}$$

and

$$R = \frac{1 + z_{em}}{1 + z_{LL}}.$$

We assume that the $\beta \leq 0.02$ systems are associated with either the quasar itself or the cluster of galaxies in which the quasar sits, and are not a function of redshift. In fact, in the ground-based sample, there are eight LLSs with $\beta \leq 0.02$ in 52 QSOs, so that in 20 QSOs observed with *IUE* one would expect three such systems. Only one lower redshift LLS has $\beta \leq 0.02$, Q0957+561, consistent with this prediction. The low-redshift sample is too small to test independently whether the $\beta \leq 0.02$ absorbers are bound to the QSO or participating in the Hubble expansion.

The distribution of systems with $\beta \geq 0.02$ is well described by a population of intervening absorbers whose comoving density is constant with epoch (Tytler 1982). The analysis of the distribution of optically thick LLSs is complicated by the fact that once a Lyman limit in a particular object is observed at z_{LL} with zero net signal beyond the edge, no other LLS can be observed in that object for $z < z_{LL}$. Following Tytler (1982), for a random distribution of absorbers, the observed density per unit X is given by

$$f(X) = \lambda \exp(-\lambda X),$$

where $\lambda(X)$ is the density per unit redshift of the parent population of LLSs, and

$$X = \int_{z_{em}}^{z} (1 + z')(1 + 2q_0 z')dz'$$

is the proper distance between z and z_{em}. The value of z is either the redshift of an observed LLS or the redshift a LLS would have at the lowest observed wavelength. Then the maximum likelihood method can be used to estimate the mean free path of LLSs at $z = 0$, in units of c/H_0:

$$\lambda_0 = \frac{m}{\sum_i x_i}$$

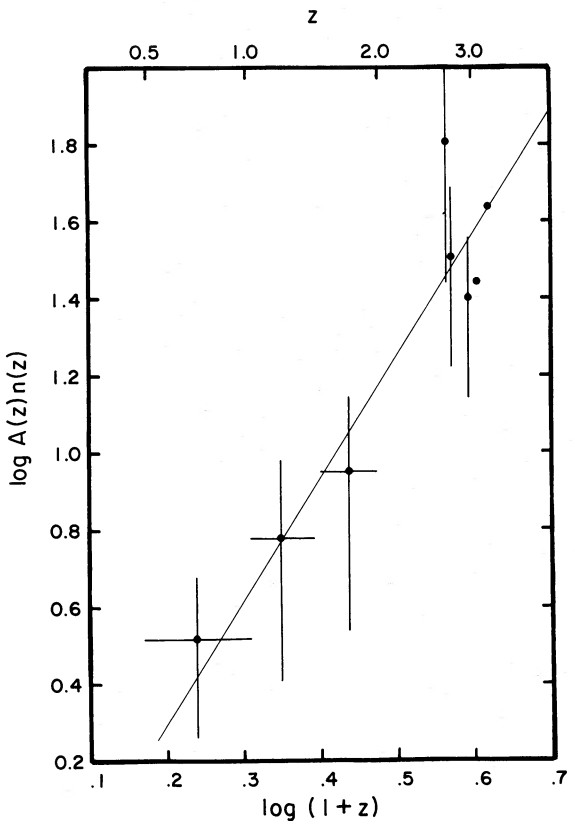

FIG. 5.—Inverse of the mean free path for Lyman limit systems, $A(z)n(z)$, as a function of redshift. The solid line is the relation expected for no evolution with epoch, i.e., constant comoving cross-sectional area of each absorber and constant comoving density of absorbers.

with an uncertainty

$$\sigma(\lambda_0) = \frac{\lambda_0}{\{\sum_i [1 - \exp(-\lambda_0 x_i)]\}^{1/2}},$$

where m is the total number of LLSs, and the sum is over the i quasars in the sample. For $q_0 = 0$, our sample yields $\lambda_0 = 0.435 \pm 0.102$, and for $q_0 = \frac{1}{2}$, $\lambda_0 = 0.758 \pm 0.179$.

In Figure 5 we plot the inverse of the mean free path to absorbers, $A(z)n(z)$, as a function of redshift, for $q_0 = 0$, where we have binned the data into discrete redshift bins, Δz. If a redshift interval contains n_q lines of sight passing through it and n_a observed absorbers, then

$$A(z)n(z) = \frac{n_a}{n_q}\frac{1}{l(\Delta z)},$$

where $l(\Delta z)$ is the proper distance corresponding to Δz; $A(z)$ represents the comoving cross section of a cloud to absorption; and $n(z)$ represents the comoving number density of absorbers. The values for $A(z)n(z)$ are tabulated in Table 7. A least squares fit to the data yields a slope of 3.3 ± 1.4. This agrees well with the relation $A(z)n(z) \propto (1+z)^3$ expected for a population of absorbers whose cross-sectional area and comoving space density are independent of z.

These Lyman limit absorbers represent only a small fraction of all observed narrow Lyman-alpha absorption lines. The total number density of Lyman-alpha lines stronger than rest equivalent width W_{λ_0} is given by

$$T_{W_{\lambda_0}}(z) = \int_{W_{\lambda_0}}^{\infty} N(W)dz,$$

TABLE 7

DISTRIBUTION OF LYMAN LIMIT ABSORBERS

(a)	(b)	(c)	(d)
0.50–1.00	6	3	0.48
1.00–1.50	5	3	0.78
1.50–2.00	5	3	0.95
2.68–2.70	31	3	1.82
2.70–2.80	17	4	1.52
2.80–3.00	15	5	1.40
3.00–3.10	6	1	1.44
3.10–3.30	2	1	1.64

(a) Redshift interval, Δz.
(b) Number of lines of sight passing through Δz, n_q.
(c) Number of observed absorbers, n_a.
(d) Log $A(z)n(z)$, see text.

where

$$N(W) = N^*/W^* \exp(-W/W^*)$$

is the spectrum of equivalent widths, $N^* = 154 \pm 11$ at $z = 2.44$, and $W^* = 0.362 \pm 0.02$ (Sargent *et al.* 1980). We can account for the observed density of optically thick Lyman limits if all Lyman lines with rest equivalent width greater than 1.7 Å show corresponding optically thick Lyman edges. This is approximately the equivalent width above which the Lyman-alpha systems with associated metal lines dominate the observed population (see Fig. 2 in Sargent *et al.* 1980).

ii) *Metal Content of the Lyman Limit Absorbers*

We have looked for C IV λλ1548, 1550 or Mg II λλ2796, 2803 absorption features associated with the LLSs in our sample and have found them in all but one, the $z = 0.713$ system in PG 1718+481 (see Table 6). Thus, these absorbers are metal-containing systems, probably associated, as discussed below, with galaxy halos. The criterion for selection in this sample, that $N(\text{H I}) \geq 2 \times 10^{17}$ cm^{-2}, differs from that of surveys for C IV or Mg II doublets (e.g., Weymann *et al.* 1979) which look for lines stronger than some limiting equivalent width. We also observe occasional strong C IV systems (see Table 6) which have no corresponding Lyman limit in the UV. This is evidence that the ionization state and temperature of the absorbing material is complex and may vary significantly from cloud to cloud at a given redshift.

Since the optical depth at the Lyman limit yields $N(\text{H I})$, the column density of neutral hydrogen, and the C IV and Mg II doublet ratios yield column densities of C IV and Mg II, respectively (Strömgren 1948; Spitzer 1968), one can measure $N(\text{Mg II})/N(\text{H I})$ and $N(\text{C IV})/N(\text{H I})$. These are tabulated in Table 6. Using these results to determine magnesium and carbon abundances depends critically on the ambient UV radiation field, which governs the ionization state of the gas. If the diffuse UV affecting gas far from the disk of a galaxy (see below) is from integrated QSO light, then ionization equilibrium models can be constructed as functions of elemental abundance and ionization parameter with a reasonably well-determined spectral shape. Complications arise in the interpretation because of the possibility of collisional ionization at high cloud kinetic temperatures and of a significant contribution of low-energy ionizing flux, particularly longward of the Lyman edge, by any nearby, actively star-forming galaxy. In addition, the small fractions of hydrogen

and magnesium found as H I and Mg II offer only weak leverage for deriving total abundances. A knowledge of the ionizing photon density and the cloud kinetic temperature is necessary for a unique solution.

The doublet ratio also can be used to derive $b = (kT/m)^{1/2}$, on the assumption that the absorption arises in gas with a single velocity component, although small errors in the doublet ratio result in large errors in b (Strömgren 1948). The b-values are listed in Table 6 and are approximately 30 km s^{-1} for the Mg II systems and 45 km s^{-1} for the C IV systems. This implies that if b truly reflects the kinetic temperature of the absorbing gas, then the two types of systems are arising from gas of similar temperature, 10^6 K. However, since the lines are unresolved, and the temperatures implied unreasonably large, these b-values instead reflect turbulent velocities of several small, cooler clouds within each system. Then the difference in b-values between C IV and Mg II reflects a difference in the velocity dispersion or scale height of the C IV clouds relative to the Mg II clouds. This is roughly what is expected if the Mg II absorption arises in low-latitude gas, and the high-ionization C IV arises in higher halo gas, as seems to be the case in our Galaxy (York 1982; Pettini and West 1982). The sample, however, is small, and the uncertainties are large.

Under the assumption that the LLSs are associated with galaxies, from the observed mean free path and the space density of galaxies, one can derive the effective cross section of a galaxy to Lyman limit absorption (Burbidge *et al.* 1977; Weymann *et al.* 1979). The mean free path of a Lyman continuum photon, l_0, is related to R^*, the effective radius an L^* galaxy must have to account for the observed line-of-sight distribution, by

$$l_0^{-1} = f \int_0^\infty \sigma dn = f\pi R^{*2}\phi_0{}^2\Gamma(0.55)\ \mathrm{Mpc}^{-1}\ ,$$

where

$$dn = \phi_0{}^* \left(\frac{L}{L^*}\right)^{-5/4} \exp\left(-\frac{L}{L^*}\right) d\left(\frac{L}{L^*}\right)$$

is the luminosity function for galaxies (Schechter 1976); $\phi_0{}^* = 2.2 \times 10^{-3}(H_0/50)^3$ Mpc^{-3} (Felten 1978); the cross section, σ, scales with luminosity as

$$\frac{\sigma}{\pi R^{*2}} = \left(\frac{L}{L^*}\right)^{0.8}$$

(Weymann *et al.* 1979), and f is the fraction of all galaxies which have absorbing gas. Then

$$R^* = \left(\frac{89.3}{l_0 f}\right)^{1/2} \left(\frac{H_0}{50}\right)^{-3/2} \left(\frac{\phi_0{}^*}{2.2 \times 10^{-3}}\right)^{-1/2} \mathrm{Mpc}\ .$$

The radius R^* is listed in Table 8, and for $\frac{1}{2} \leq f \leq 1$, and $50 \leq H_0 \leq 85$ km s^{-1} Mpc^{-1}, and $0 \leq q_0 \leq \frac{1}{2}$, R^* takes on values between $6R_H$ and $10R_H$, where R_H is the Holmberg radius of an L^* galaxy, about 16 kpc (Mihalas and Binney 1981). By comparison, in the survey of Weymann *et al.* (1979), the C IV systems and Mg II systems had mean free paths which implied $R^* = 2$–$6R_H$ for the same parameters (see Table 8). The interpretation of this difference in terms of a physical model for the distribution of absorbing material in a typical galaxy is complicated, since not all C IV systems have Lyman limits, and not all Lyman limits have observable metal lines, presumably resulting from variations in ionization states and abundances from cloud to cloud. The indication, however, is that Lyman limits are generally produced at lower total column densities than metal doublets; in fact, the metal lines we observe (Table 6) are often weaker than those included in complete metal doublet surveys. Moreover, the Lyman limit systems, like the metal-line absorption systems, seem too numerous to be due to normal disks of galaxies but may instead arise from extended halos. Since we are sensitive to $N(\mathrm{H\ I}) \geq 2 \times 10^{17}$ cm^{-2}, which is substantially lower than limiting column densities achieved in typical 21 cm surveys of galaxies, this is not surprising. A recent study of Briggs (1982) of H I in the outer regions of a complete sample of nearby spirals found little 21 cm emission beyond $3R_H$ in any galaxy, but was only sensitive to $N(\mathrm{H\ I}) \geq 10^{18}$ cm^{-2}.

TABLE 8

MEAN FREE PATHS FOR ABSORPTION

Parameter	$l_0 h$ (Mpc)[a]	$R^* h^{-3/2} F^{-1/2}$ (kpc)[b]
Lyman limits, $q_0 = 0$	2610 ± 612	262 (+37, −27)
Lyman limits, $q_0 = \frac{1}{2}$	4548 ± 1072	198 (+29, −20)
C IV, $q_0 = 0$	18100[c]	100
Mg II, $q_0 = 0$	43200[c]	64

[a] $h = H_0/50$ km s^{-1} Mpc^{-1}.
[b] $F = f/0.5$ (see text).
[c] Weymann *et al.* 1979.

IV. SUMMARY

We have studied the spectral energy distributions in nine high-redshift quasars, in the observed wavelength range 1250–10000 Å. The main results are the following.

1. The spectral energy distributions steepen shortward of about 1200 Å in all but one object. The amount of observed steepening increases with increasing redshift but is uncorrelated with QSO luminosity, suggesting that it arises from absorption by intervening material along the line of sight.

2. In the QSOs with high enough redshift that Lyman-alpha can be observed at high resolution from the ground, we can account for the observed continuum steepening by the Lyman continuum absorption corresponding to the narrow Lyman-alpha absorption lines we see. The steepening is caused by four to eight absorbers, or the strongest 5% of the Lyman-alpha lines, if their Doppler widths are $20 \leq b \leq 50$ km s^{-1}, with implied optical depths at the Lyman limit of about 0.1. These absorbers can probably be identified with the low column density tail of the metal-containing galactic halo population, rather than the high column density end of the Lyman-alpha forest.

3. Reddening may contribute to the steepening of the QSO continua, if dust lies along our line of sight to the continuum source, and is difficult to assess quantitatively.

4. Intrinsic steepening cannot be ruled out in any particular object but is difficult to model precisely because of the contribution of absorption and reddening to the spectral steepening. When high-resolution, high signal-to-noise spectra shortward of Lyman-alpha become available, it will be possible to correct for the Lyman continuum absorption, either by direct measurement of the Lyman discontinuities themselves or by measurement of column densities from line profiles of the Lyman series.

5. The depression of the continua between Lyman-alpha and Lyman-beta compared with longer wavelengths, if attribu-

table to narrow-line Lyman-alpha absorption, implies moderate density evolution of the Lyman-alpha forest between $z = 1$ and $z = 3.5$, with $dN/dz \propto (1 + z)^{\gamma}$ and $\gamma = 1.29 \pm 0.20$.

6. Optically thick Lyman limit discontinuities are seen with $z_{abs} \ll z_{em}$. In eight out of nine systems, associated Mg II or C IV doublets are observed. Combining this sample with high-redshift QSOs observed from the ground, it is shown that statistically, these absorbers are well described by a population of intervening objects, whose comoving density is constant with epoch. To account for the distribution we see, an L^* galaxy must have a cross section to absorption of 5–10 Holmberg radii.

We are grateful for the allocations of observing time and excellent technical assistance by the staffs of the *International Ultraviolet Explorer*, Palomar, Steward, and Multiple Mirror Telescope observatories. We acknowledge helpful guidance in *IUE* observing by A. L. Lane, and useful discussions with F. H. Chaffee, Jr. This work was supported in part by NASA grants NAG 5-38 and NAS 7-100, and NSF grant 8109025.

REFERENCES

Boggess, A., *et al.* 1978*a*, *Nature*, **275**, 372.
———. 1978*b*, *Nature*, **275**, 377.
Bohlin, R. C. 1978, *Ap. J.*, **224**, 132.
Bohlin, R. C., Holm, A. V., Savage, B. D., Snijders, M. A. J., and Sparks, W. M. 1980, *Astr. Ap.*, **85**, 1.
Boksenberg, A., and Snijders, M. A. J. 1981, *M.N.R.A.S.*, **194**, 353.
Boroson, T., Sargent, W. L. W., Boksenberg, A., and Carswell, R. F. 1978, *Ap. J.*, **220**, 772.
Briggs, F. H. 1982, in *The Comparative* H I *Content of Normal Galaxies: A Green Bank Workshop*, ed. M. Haynes and R. Giovanelli (Green Bank, W. Va.: Publications Division of NRAO), p. 50.
Burbidge, G., O'Dell, S. L., Roberts, D. H., and Smith, H. E. 1977, *Ap. J.*, **218**, 33.
Canfield, R. C., and Puetter, R. C. 1980, *Ap. J.* (*Letters*), **236**, L7.
———. 1981, *Ap. J.*, **243**, 390.
Carswell, R. F., Morton, D. C., Smith, M. G., Stockton, A. N., Turnshek, D. A., and Weymann, R. J. 1984, *Ap. J.*, **278**, 486.
Chaffee, F. 1982, private communication.
Davidson, K., and Netzer, H. 1979, *Rev. Mod. Phys.*, **51**, 715.
Dean, A. J., and Ramsden, D. 1981, *Phil. Trans. Roy. Soc. London, A*, **301**, 577.
Eastman, R. G., MacAlpine, G. M., and Richstone, D. O. 1983, *Ap. J.*, **275**, 53.
Elvis, M., and Fabbiano, G. 1982, in *Advances in Ultraviolet Astronomy: Four Years of IUE Research*, ed. Y. Kondo, J. M. Mead, and R. D. Chapman (NASA CP-2238), p. 205.
Felten, J. E. 1978, *A.J.*, **82**, 861.
Ferland, G. J., and Netzer, H. 1979, *Ap. J.*, **229**, 274.
Grandi, S. A. 1983, *Ap. J.*, **268**, 591.
Green, R. F., Bechtold, J., Weymann, R. J., and Chaffee, F. H., Jr. 1983, *Bull. AAS*, **14**, 908.
Green, R. F., Pier, J. R., Schmidt, M., Estabrook, F. B., Lane, A. L., and Wahlquist, H. D. 1980, *Ap. J.*, **239**, 483.
Gunn, J. E., and Peterson, B. A. 1965, *Ap. J.*, **142**, 1633.
Heiles, C. 1975, *Astr. Ap. Suppl.*, **20**, 37.
Jones, T. W., O'Dell, S. L., and Stein, W. A. 1974*a*, *Ap. J.*, **188**, 353.
———. 1974*b*, *Ap. J.*, **192**, 261.
Kwan, J., and Krolik, J. H. 1981, *Ap. J.*, **250**, 478.
Latham, D. 1982, in *IAU Colloquium 67, Instrumentation for Astronomy with Large Optical Telescopes*, ed. C. Humphries (Dordrecht: Reidel), p. 245.
Lynden-Bell, D. 1969, *Nature*, **233**, 690.
MacAlpine, G. M. 1981, *Ap. J.*, **251**, 465.
MacAlpine, G. M., and Feldman, F. 1982, *Ap. J.*, **261**, 421.
Malkan, M. A. 1983, *Ap. J.*, **268**, 582.
Malkan, M. A., and Sargent, W. L. W. 1982, *Ap. J.*, **254**, 22.
Mathews, W. G., Blumenthal, G. R., and Grandi, S. A. 1980, *Ap. J.*, **235**, 971.
Mihalas, D., and Binney, J. 1981, *Galactic Astronomy: Structure and Kinematics* (2d ed.; San Francisco: Freeman and Co).
Morton, W. A., and Morton, D. C. 1972, *Ap. J.*, **178**, 607.
Mushotzky, R., and Ferland, G. J. 1984, **278**, 558.
Netzer, H., and Davidson, K. 1979, *M.N.R.A.S.*, **187**, 871.
Oke, J. B., 1969, *Pub. A.S.P.*, **81**, 11.
Oke, J. B., and Gunn, J. E. 1983, private communication.
Oke, J. B., and Korycansky, D. G. 1982, *Ap. J.*, **255**, 11.
Ostriker, J. P., and Cowie, L. L. 1981, *Ap. J.* (*Letters*), **243**, L127.
Ostriker, J. P., and Heisler, J. 1984, *Ap. J.*, **278**, 1.
Ostriker, J. P., and Ikeuchi, I. 1983, *Ap. J.* (*Letters*), **268**, L63.
Peterson, B. A. 1983, in *IAU Symposium 104, Early Evolution of the Universe and Its Present Structure*, ed. G. Chincarini and G. Abell (Dordrecht: Reidel), p. 349.
Pettini, M., and West, K. A. 1982, *Ap. J.*, **260**, 561.
Puetter, R. C., Burbidge, E. M., Smith, H. E., and Stein, W. A. 1982, *Ap. J.*, **257**, 487.
Richstone, D. O., and Schmidt, M. 1980, *Ap. J.*, **235**, 377.
Robertson, J. G., Shaver, P. A., and Carswell, R. F. 1983, preprint.
Roser, H., *et al.* 1983, in preparation.
Sargent, W. L. W., Young, P. J., Boksenberg, A., and Tytler, D. 1980, *Ap. J. Suppl.*, **42**, 41.
Schechter, P. L. 1976, *Ap. J.*, **203**, 297.
Schmidt, M., and Green, R. F. 1983, *Ap. J.*, **269**, 352.
Seaton, M. J. 1979, *M.N.R.A.S.*, **187**, 73P.
Shields, G. A. 1978, *Nature*, **272**, 706.
Shuder, J. M., and MacAlpine, G. M. 1979, *Ap. J.*, **230**, 348.
Smith, M. G., *et al.* 1981, *M.N.R.A.S.*, **195**, 437.
Snijders, M. A. J. 1980, *Second European IUE Conference, Tubigen* (ESA SP-157), p. lxxi.
Spitzer, L. 1968, *Diffuse Matter in Space* (New York: Interscience).
Strömgren, B. 1948, *Ap. J.*, **108**, 242.
Tananbaum, H., *et al.* 1979, *Ap. J.* (*Letters*), **234**, L9.
Turnrose, B. E., and Perry, P. M. 1977, *IUE Image Processing Overview* (Silver Springs, Md.: Computer Sciences Corporation, NASA/Goddard Space Flight Center).
Tytler, D. 1982, *Nature*, **298**, 427.
Usher, P. D., Warnock, A., III, and Green, R. F. 1983, *Ap. J.*, **269**, 73.
Weisheit, J. C., Shields, G. A., and Tarter, C. B. 1981, *Ap. J.*, **245**, 406.
Weymann, R. J., Williams, R. E., Peterson, B. M., and Turnshek, D. A. 1979, *Ap. J.*, **234**, 33.
York, D. 1982, *Ann. Rev. Astr. Ap.*, **20**, 221.
Young, P. J., Sargent, W. L. W., and Boksenberg, A. 1982*a*, *Ap. J.*, **252**, 10.
———. 1982*b*, *Ap. Ap. Suppl.*, **48**, 445.
Zamorani, G., *et al.* 1981, *Ap. J.*, **245**, 357.

JILL BECHTOLD and RAY J. WEYMANN: Steward Observatory, University of Arizona, Tucson, AZ 85721

FRANK B. ESTABROOK, RICHARD D. SHERMAN, and HUGO D. WAHLQUIST: Jet Propulsion Laboratory, California Institute of Technology, 4800 Oak Grove Dr., Pasadena, CA 91103

RICHARD F. GREEN: Kitt Peak National Observatory, Box 26732, Tucson, AZ 85726

T. M. HECKMAN: Astronomy Program, University of Maryland, Space Sciences Bldg., College Park, MD 20742

MAARTEN SCHMIDT: Department of Astronomy 105-24, California Institute of Technology, Pasadena, CA 91125